JOURNAL OF SPACECRAFT AND ROCKETS
Vol. 45, No. 4, July–August 2008

Enhancement of Emissive Properties for In-Space High-Temperature Radiator Materials

Ivana A. Hrbud*
Purdue University, West Lafayette, Indiana 47907

DOI: 10.2514/1.31101

This study investigates emissive properties as a function of time and temperature of niobium and tantalum, for which the surfaces have been altered by an arc-texturing technique. To date, space radiators achieve relatively high emissivity at moderate temperature with specially developed paints and coatings. The emissive performance of arc-textured surfaces is compared with the emissive capability of untreated and sandblasted surfaces at temperatures of 1300 and 1700 K. Arc-texturing produces surfaces with emissivity coefficients between 0.6 and 0.9, which translates into an enhancement of about two to four times when compared with untreated or sandblasted samples. Material characterization techniques such as optical microscopy, scanning electron microscopy, stylus-type prolifometry, energy-dispersive x-ray spectroscopy, and x-ray diffractometry are employed to study the geometric topology of altered surfaces. These techniques assist in unlocking the mechanisms that are ultimately responsible for emissivity behavior as a function of time and temperature and that consequently lead to manufacturing processes of desirable morphologies.

Nomenclature

A	=	surface area, cm^2
a	=	cross-sectional area, cm^2
I	=	current, A
k	=	thermal conductivity, $W \cdot m^{-1}\ K^{-1}$
P	=	power, W
R	=	resistance, Ω
T	=	temperature, K
V	=	voltage, V
$\Delta T/\Delta x$	=	temperature gradient, K/cm
ε	=	emissivity
σ	=	Stefan–Boltzmann constant, kg/m^3 $(5.670 \times 10^{-8}\ W \cdot m^{-2}\ K^{-4})$

Subscripts

cond	=	conductive
conv	=	convective
emis	=	emissive
env	=	environment
ohmic	=	ohmic heating
S	=	surface

I. Introduction

THERMAL management has been a major design issue of spacecraft since the dawn of space flight. Because thermal heat has to be dissipated without the presence of intermediate matter, radiative heat transfer of energy compensates for the lack of convection and conduction. Over the past 50 years, ever-more-ambitious missions, human and robotic, have pushed the demand for electric power production, which inadvertently results in generating large amounts of waste heat. Power generation, demanded by industry, military, and government agencies, has seen an enormous technological evolution over the past two decades. Research and development has produced significant advancements regarding energy production (such as high-voltage/high-power solar arrays and concentrators [1–3]) and energy storage (such as lithium-ion batteries [4] and fuel cells [5]). Just in the past decade, nuclear space reactor and energy conversion technologies [6] have seen resurgence in research and technology development [7].

The need to efficiently dissipate large amounts of waste thermal heat is prevalent in current missions and will be more so in the future. As with any spacecraft, weight and weight reduction are commanding design characteristics upon which many other considerations and characteristics depend. According to the Stefan–Boltzmann law, the energy radiated from a body's surface depends on the size of the radiating surface, the temperature (to the fourth power) at which the surface is operated, and the emissivity of the surface [8]. Emissivity is a measure of how well the real surface of a body radiates energy when compared with the energy radiated by a blackbody at the same temperature. The size of a space radiator (and, consequently, weight, volume, and cost) is a strong function of operating temperature and emissive capability of the surface. The goal of designing thermal management control is to maximize the operating temperature of the radiator to take advantage of the temperature's exponential influence on the Stefan–Boltzmann law. In addition, the emissivity of a surface has a linear effect in reducing the required area of radiators and, consequently, a high value is desirable. To date, radiators achieve relatively high emissivity at moderate temperature with specially developed paints and coatings [9–12]. These surfaces are sensitive to degradation effects such as thermal cycling, UV radiation, atomic oxygen exposure, and other space environmental effects [13,14]. These coating represent the most commonly used thermal control technique. Other techniques include droplet, liquid film, and belt radiators [15–18]. Direct heat rejection into space is employed in various space applications such as nuclear reactors, nuclear thermal propulsion, solar dynamic energy generation, electric propulsion, high-power/temperature electronics, space-based weapons, Lunar and Martian surface applications, etc. [19,20].

Because the size of the radiator and its contribution to the spacecraft mass are primarily functions of temperature and emissivity, investigating surface properties of materials addresses the problem of heat dissipation. Radiative properties of metal surfaces include absorption, reflection, and emission. Emission occurs from any surface that is at a finite temperature and is associated with the emissivity of the material surface. The emitting ability depends on factors such as body temperature, emission wavelength (spectral vs total), emission angle (directional vs hemispherical) [8], and roughness of the surface. A major problem when predicting radiative properties is the definition of surface

Received 21 October 2007; accepted for publication 27 February 2008.

*Assistant Professor, Purdue University, School of Aeronautics and Astronautics, 701 West Stadium Avenue. Member AIAA.

characteristics required for analytical calculations. One of these characteristics is surface roughness. Edwards and Catton [21] provided a detailed comparison of several mechanical treatment techniques and its effects on emissive properties for aluminum, titanium, and stainless steel. These texturing methods enhance and increase spectral emissivity at individual wavelengths between the infrared and visible region. The degree of roughness and roughness morphology plays a significant role in the emissive properties of tungsten [22]. Surface morphology is reduced to conical and cylindrical cavities in an attempt to apply analytical modeling and to predict emissivity as a function of form and dimension [23].

To satisfy demands on high performance, requirements for surface quality and property sparked exploration of innovative techniques to meet specific needs. Ion-beam texturing [24], discharge chamber texturing [25], and carbon arc electric discharge [26] are some of the techniques used on high-temperature materials in recent years. The ion-beam texturing technique produces morphologies with conical structures. They have a uniform distribution over the surface and are similar in form and dimensions. This surface-altering method yields significant enhancement of emissive properties when compared with untreated samples. The steep walls of the cones render a surface highly absorptive because radiation is trapped in cavities by multiple reflections. According to Kirchhoff's law, emissivity is equal to absorptivity [8]. High-temperature emission is promoted because this texturing technique favors emissivity enhancement in the visible range of the electromagnetic spectrum. Carbon arc-texturing alters the surface morphology by striking an electrical arc discharge across the surface and producing a microscopically rough surface. These techniques have the potential to engineer integrated emissive properties of radiator materials.

This paper summarizes the experimental findings and performance characteristics of arc-textured high-temperature radiator materials. The main objectives of this research were to experimentally determine emissive properties, investigate high-temperature stability, and identify likely mechanisms contributing to the enhancement of radiative capability. Correlating experimental data, parameters controlling the arc-texturing process, and mechanisms responsible for emissivity increase will yield the blueprint for producing engineered integrated surfaces that will meet the specific needs of ever-more-demanding mission scenarios.

II. Apparatus and Experiment

One of the main objectives of this research is to experimentally evaluate emissive properties of high-temperature materials such as tantalum and niobium as possible candidates for space radiators. Primarily, experiments intend to reveal the hemispherical total emissivity as a function of time for these materials for which the surfaces are subjected to arc-texturing and sandblasting. The experiment philosophy is based on the Stefan–Boltzmann law and exploits the resistive nature of metals. Ohmic heating provides an elegant solution to control the power input and, consequently, the temperature of a sample to a very high degree. That power input is directly linked to the current though the sample and the voltage drop across two distinct locations along the sample. These two locations for the voltage tab also determine the area through which the electric power is radiated. A thermocouple measures the surface temperature of the sample. It is welded midway between the voltage tabs. The hemispherical total emissivity is calculated purely from measured parameters (temperature, voltage, current, and area). Untreated tantalum and niobium samples will undergo similar heating tests to establish a baseline for comparison. Arc-texturing and sandblasting alter the surface morphology of materials and thus change the optical characteristics of the surface. The experimental apparatus consists of a vacuum chamber, high-current power supply, water-cooling system, and diagnostics. Figure 1 illustrates the testing apparatus for the heating experiments. The following sections describe the test facility and its support system in which the samples are tested, the power supply for the heating of the samples, diagnostics to obtain critical test data from which emissivity is calculated, and the experimental procedure to which all samples are subjected.

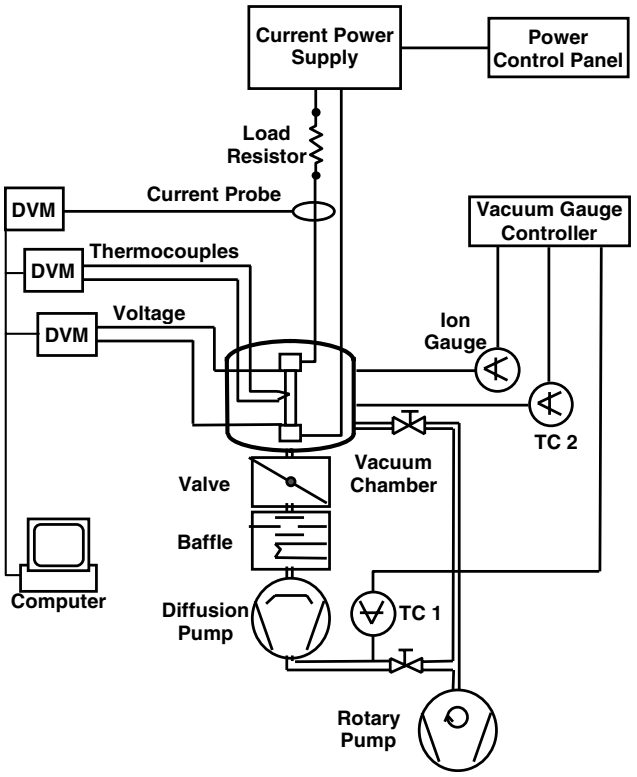

Fig. 1 Schematic of the test apparatus.

A. Testing Facility

The testing facility consists of a vacuum system, a water-cooling system, and pressure-monitoring devices. Heating experiments were conducted in a stainless steel chamber. The vacuum chamber has the shape of a cube, for which each side is approximately 50 cm. In addition to an access door, which is the size of one face, the vessel features three 36-cm O-ring-sealed flanges. An oil diffusion pump rated at a pumping speed of 2800 l/s provides vacuum pressures in the lower 10^{-4}-Pa range, and a mechanical pump provides the backup pumping for proper operation of the vacuum system. An ion gauge and a thermocouple gauge monitor the pressure in the vacuum chamber. A second thermocouple gauge is located in the foreline and takes readings close to the intake of the mechanical pump.

Because of the nature of the experiment, a water-cooling system is integrated inside the vacuum chamber. The coolant conducts away absorbed energy and keeps crucial components at a constant temperature. The cooling system circulates water through a shroud and heating electrodes. The heating electrodes that clamp the test article are made of copper. The test operating temperature (1000–2000 K) exceeds the melting temperature of copper (1358 K). A cooling shroud in the form of two panels surrounds the hot test article. The panels absorb and conduct away the radiated energy from the sample during the experiment. The interior walls of the vacuum chamber do not heat up and, consequently, do not reemit absorbed energy back to the test article, which could affect the energy balance. Panel surfaces facing the test article are painted with a high-temperature black paint. In addition, the panels are slightly curved. Reflection of emitted energy by the test article is suppressed and a high absorption rate is ensured. Figure 2 illustrates the schematic of the water-cooling system.

B. Power Supply

Ohmic heating of test articles affords a broad range of experiment temperatures. A welding power supply delivers the current for the electrical resistive heating of the samples. The unit is a high-current power source consisting of a three-phase transformer and sealed selenium/silicon rectifiers to produce dc power. Preliminary tests were necessary to determine proper circuit configuration to adopt the current output and current control to the specific needs of the

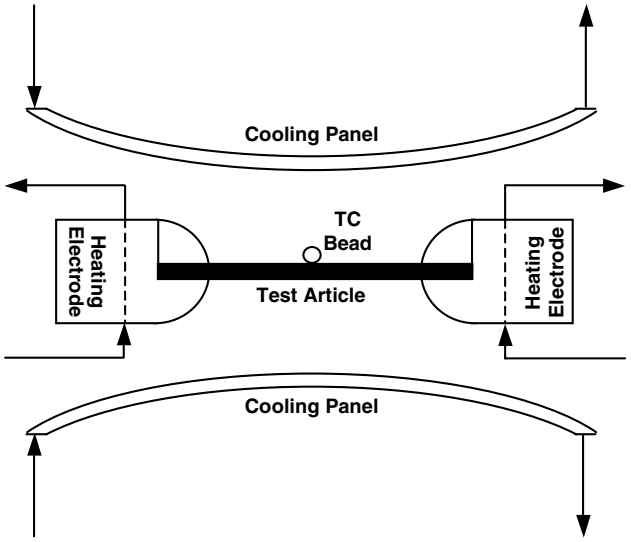

Fig. 2 Schematic of the water-cooling system.

experiment. A major part of the modification includes a load resistor in series to the resistance of the sample. The load resistor consists of four 125-mΩ resistors wired in parallel, with each capable of dissipating up to 500 W. This configuration results in a resistance of 31.25 mΩ. The resistance of a sample is estimated based on geometric dimensions and a temperature/material-dependent resistivity. For the anticipated experimental temperature range (1000–2000 K), sample resistance varies between 14 and 25 mΩ. After the modifications, the current encompasses a range from 40 to 250 A, which represents a power output of up to 4300 W. This allows a wide temperature range for both tantalum and niobium. The control panel of the welding power supply consists of a current readout and current control knob.

Two heavy-gague welding cables connect the power supply to two high-power feedthroughs, which are installed on the top face of the vacuum chamber. Inside the vacuum chamber, another two welding cables connect the feedthroughs with the heating electrodes. A sample is placed between the heating electrodes closing the electrical circuit.

C. Diagnostics

The tungsten/rhenium thermocouple (TC) measures the actual surface temperature of the heated samples. This thermocouple combination was chosen for its high-temperature operating range, even though this TC is sensitive to embrittlement and thermal stress. Thermocouples exploit a voltage difference, which is induced by dissimilar metals when exposed to a temperature gradient, for determining the temperature of an object. A digital voltage meter (DVM) measures and displays this voltage, which is later converted to a temperature. A series of initial tests was conducted to determine the appropriate TC size and to establish the proper configuration and installation procedure for this experiment. Preliminary tests showed that the original TC bead size led to local cooling of the sample where the TC attached to the sample. The thickness of the sample is 0.254 mm, which was the diameter of an individual TC wire. The resulting diameter of the TC bead was about three times the sample thickness and, consequently, represented a heat sink. To eliminate this effect, the diameter of the TC wire was reduced to 76.2 μm. To ensure good physical contact, the thermocouple is welded to the sample surface with a small spot-welding device. The location of the TC bead is in the middle of the sample with respect to the length and width. Before and after each heating experiment, the condition of each TC junction on the sample surface was examined by using a microscope. Any separation between the TC wires will affect the accuracy of the temperature measurement. Direct current passing through a resistor will cause a voltage drop across that resistor. A voltage drop can be measured along the resistor at any position and between any two points and is a function of material resistivity, current, and point separation. Thus, any separation between the TC wires picks up a voltage-drop measurement, superimposes it, and taints the temperature measurement.

Electric power is delivered to the sample and raises the temperature of the sample based on its resistive properties. Inside the vacuum chamber, voltage probes connect to the opposite ends of the sample at a known distance apart. They are led through an instrumentation feedthrough to a DVM, which measures and displays the voltage drop across the sample. A current probe measures the current through the circuit and provides its data to another DVM for display.

D. Experimental Procedure

A sample (treated or untreated) is carefully placed between the heating electrodes. Careful handling of all samples is important to maintain comparable testing conditions and to minimize unintended (uncontrollable) contamination of the samples. Setscrews secure the sample and provide excellent physical contact to the heating electrodes. The best TC welding junction resulted from welding only one TC wire to the sample surface and then attaching the other on top of the first. During this process, a microscope is used to examine the TC bead. Once it passes inspection, the sample is placed in the vacuum chamber between the cooling panels. The heating electrodes are then connected to the water-cooling system and the high-current feedthrough. Before the vacuum chamber is closed, the water-cooling system undergoes a leak check and diagnostics leads are connected to the appropriate feedthroughs. The vacuum chamber is closed and pumped down. Once the 10^{-4}-Pa range is obtained, the heating experiment starts. All diagnostics units are in the on position and data logging commences. Turning the current control knob increases the current in the circuit. Over a 20-min period, the current increase is slow, to avoid unnecessary thermal stress between the sample and TC bead. Once the desired temperature (1300 or 1700 K) is reached, heating experiments last between 4 and 12 h for both textured and untreated samples. During the first 4 h, data points are recorded every 5 min. After that, the interval between two measurements increases to 10 min. Data logging includes vacuum pressure (ion gauge), voltage drop across the sample, current, and TC temperature. Reaching a desired heating duration (4, 8, or 12 h) completes the experiment for the sample. The current is slowly reduced over a period of 5 min. All diagnostics and support systems are turned off, whereas the water-cooling system remains running until certain components have cooled sufficiently. The vacuum system is returned to atmospheric pressure, which allows removal of the sample. The sample is stored and cataloged and undergoes surface morphology characterization.

III. Analytical Technique: Emissivity Calculation

One main objective of this investigation is to experimentally determine the total hemispherical emissivity of candidate radiator materials for which the surface morphology is altered. Emissivity is a measure of how much energy is radiated by a body when compared with the energy radiated by a blackbody at the same temperature. Emissivity is a strong function of temperature, emission angle (directional vs hemispherical), and wavelength (spectral vs total). The control of vital input parameters and a carefully executed analysis drive experiment design and diagnostics. The following analysis and calculation procedure of the total hemispherical emissivity were adopted in accordance with [27].

A power balance analysis performed on the sample takes into account all sources of power input and output, which will influence heating (and, consequently, the temperature) of the sample:

$$P_{\text{in}} = P_{\text{out}} \qquad P_{\text{ohmic}} + P_{\text{env}} = P_{\text{emis}} + P_{\text{cond}} + P_{\text{conv}} \tag{1}$$

The total heat input to the sample consists of heat generated by resistance due to electric current and radiant energy incident to the sample that is absorbed. The total heat output encompasses the emitted energy by the hot sample, heat loss by conduction and convection through the environment, and heat conducted away through the ends of the sample, thermocouples, and potential leads.

Ohmic heating of an object provides an eloquent method to control and determine the power input with high certainty, simply by taking advantage of the object's resistivity. Electric current passing through a resistor generates thermal energy according to

$$P_{\text{ohmic}} = R \cdot I^2 = V \cdot I \tag{2}$$

A DVM measures the voltage drop across the sample, whereas a current probe determines the current through the sample. The other contribution to input power takes into account radiative, conductive, and convective heat transfer by the environment, which includes vacuum chamber walls, cooling panels, gas environment, and heating electrodes. Because the experiment is executed in a vacuum chamber at high vacuum, any energy transfer due to convection and conduction by the surrounding gas environment can be neglected. The heating electrodes are made of copper and are water-cooled (at significantly lower temperatures than the sample), which makes their conductive heat contribution negligible. Typically, a complete enclosure for which the walls are maintained at a uniform temperature is considered to be a blackbody radiator. The cooling panels in this experiment are convex, painted with a highly absorptive black paint, and cooled and maintained at a constant temperature (room temperature). This shroud is not a complete enclosure, but it exhibits many characteristics of a blackbody radiator. Optical characteristics of these panels absorb the radiative energy emitted by the hot sample and inhibit remittance and/or reflection of that energy. The relative large size difference between the panels and sample further accentuates the liberty to neglect this contribution. All of this also leads to an insignificant contribution to the radiative power input.

The power output accounts for radiative heat transfer by the hot sample, conductive, and convective losses. As before, conductive and convective heat losses through the atmosphere can be omitted, because the experiment is performed in vacuum. Equation (3) describes heat loss by conduction in materials:

$$P_{\text{cond}} = 2 \cdot ka \cdot \frac{\Delta T}{\Delta x} \tag{3}$$

Loss by conduction occurs through TC leads, tab leads measuring voltage drop across the sample, and the ends of the sample. The cross-sectional area of a TC wire is 4.56×10^{-5} cm^2, and the contact area of the tab attachment is estimated at 2×10^{-4} cm^2. The thermal conductivity of all the leads is a function of temperature and is conservatively estimated at about 1 W $\cdot$ cm^{-1} K^{-1}. The temperature gradient across the TC and voltage tabs is not known with a high degree of certainty. Considering a conservatively high-temperature gradient of 2000 K/cm, heat conducted away by these contacts calculates to less than 1 W. The cross-sectional areas for tantalum and niobium samples are 2.72×10^{-2} and 2.4×10^{-2} cm^2, respectively. At room temperature, the thermal conductivity for theses metals is about 0.6 W $\cdot$ cm^{-1} K^{-1}. Because the temperature gradient along the sample is uniform, variations in temperature are small in the vicinity of the voltage tabs. Considering 5 K/cm and 0.6 W $\cdot$ cm^{-1} K^{-1} (this value is lower at testing temperature), heat conducted through the ends of the samples is less than 1.44×10^{-1} W (niobium) and 1.62×10^{-1} W (tantalum). Hence, these heat losses are negligible.

The area of the sample between the voltage measurement is important and is the object of this analysis. The emitted energy by the hot sample is calculated with the Stefan–Boltzmann law according to

$$P_{\text{emis}} = \varepsilon_S \cdot \sigma \cdot A_S \cdot T_S^4 \tag{4}$$

Taking into account the preceding discussion, Eq. (1) reduces to

$$V \cdot I = \varepsilon_S \cdot \sigma \cdot A_S \cdot T_S^4 \tag{5}$$

Voltage drop between two locations is measured and determines the amount of power delivered to the sample across that distance. The area between these two locations is responsible for radiatively dissipating power, which is dictated by the emissivity and the temperature of the surface. In this study, a TC directly measures the surface temperature of the sample. Rearranging the power balance equation allows the calculation of hemispherical total emissivity, determined by experimental measurements:

$$\varepsilon_S = \frac{V \cdot I}{\sigma \cdot A_S \cdot T_S^4} \tag{6}$$

Experimental data are obtained as a function of elapsed time. The total hemispherical emissivity computes according to Eq. (6) and is plotted as a function of time, temperature, and surface condition. Evolution of emissivity with time reveals the stability and performance of engineered surfaces at high temperatures and over the operating period.

IV. Arc-Texturing and Sample Preparation

Emissive performance of a surface obtained by arc-texturing depends on many parameters: namely, arc current and voltage, current waveform (dc, ac, shape, frequency, etc.), material of the texturing electrode, textured material, and density and frequency of the arc sites. This study investigates tantalum and niobium as textured radiator materials, mainly due to their high-temperature capabilities. Emissive properties of arc-textured samples are compared against the performance of untreated and sandblasted samples, in which untreated samples form the baseline.

The materials are supplied in long strips that are 0.254 mm thick. The tantalum strip has a width of 10.7 mm, and the niobium strip has a width of 9.5 mm. All samples are trimmed to a length of about 15 cm. Two areas are marked off along that length. A smaller area (analysis area) of about 12 mm is designated for scanning electron microscopy (SEM) analysis. The other region (experiment area) is about 9 cm long and constitutes the area that is textured (arc-textured or sandblasted) on both sides of the sample.

After treatment of the designated areas, the samples are trimmed to about 11.5 cm, centered on the 9-cm-long treated length. The untreated overhang allows installation into the heating electrodes. The small area is also trimmed and stored for later analysis. Figure 3 illustrates a schematic of the sample.

A. Arc-Texturing Apparatus

The main components of the arc-texturing apparatus are a sample support, a power supply, a carbon rod, and a nitrogen-purged enclosure. The apparatus was designed and built in-house, meeting the specific needs of the present research objectives and experiment philosophy. A similar system is described by [26]. Figure 4 illustrates a schematic of the arc-texturing apparatus.

The 15-cm-long samples are secured on the sample support. The sample support is a Plexiglas tray covered by a metal mesh. The tray connects to a high-pressure nitrogen tank, and a wire connects the metal mesh to the ground terminal of an ac variable transformer (variac). The ac variac has a conventional 120-V/15-A power input and serves as a controllable power source. Turning a control knob varies the voltage output between the ground and the output terminal. A variac is the ac equivalent to a dc voltage divider. A DVM measures the potential difference between the two terminals. A wire with an alligator clamp connects the output terminal of the variac to the arc-texturing electrode. This electrode is a carbon rod for which the diameter is about 6.35 mm. A thin copper foil wraps tightly around the rod to ensure good thermal and electrical conductivity. A Plexiglas holder clamps around the electrode. The holder features a

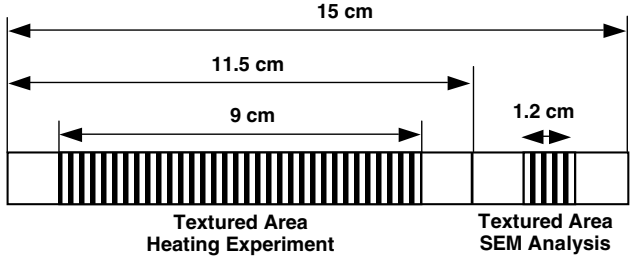

Fig. 3 Sample preparation.

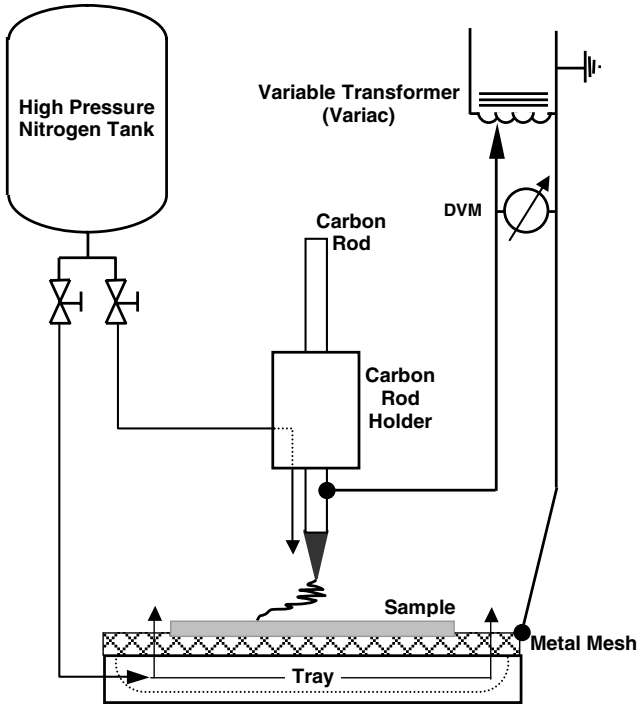

Fig. 4 Schematic of the arc-texturing apparatus.

connection to a high-pressure nitrogen tank and an exhaust orifice, which expels nitrogen gas parallel to the electrode. The sample support and electrode holder are placed in an enclosure in which the arc-texturing procedure is performed. Two round openings covered by latex rubber enable access to the interior of the enclosure. The latex covers have circular cutouts that are barely big enough for a hand to push through. The latex expands and tightly fits around the wrist of an operator. High-pressure nitrogen gas is expanded through the support and holder, cooling both the sample and electrode during the arc-texturing process. Nitrogen gas circulates through the enclosure and flushes trapped air through vent holes, which are drilled in a top corner. This provides an inert-gas environment inside the enclosure. Oxidation during the arc-texturing procedure is prevented or at least drastically reduced.

B. Preparation of Test Samples

The surface quality of a material plays a vital role in defining its optical characteristics, such as being absorptive, emissive, reflective, etc. To determine the evolution of emissive properties of candidate radiator materials, three surface morphologies are investigated. These include arc-texturing, sandblasting, and original surface conditions. The procedures outlined for the arc-texturing and sandblasting of samples were meticulously executed to ensure reproducibility and similar starting (testing) conditions.

As previously mentioned, arc-texturing depends on a variety of parameters. For this investigation, a few of those parameters were chosen and held constant for all the samples, which were treated. The variac supplies ac current at 60 Hz. The voltage between the ground (sample) and texturing electrode is set to 10 V and held constant. The texturing electrode is a round carbon rod with a 6-mm diameter. Because of arcing, the electrode tip undergoes severe erosion and necessitates periodic resharpening.

The valves on the nitrogen tank are opened. Nitrogen floods and flushes the enclosure. Inside of the enclosure, a 15-cm sample is secured on to the metal mesh of the tray. A sharpened carbon rod is placed in the holder and connected to the output terminal of the variac. The electrode is held above the sample with its tip pointing down and carefully lowered till an arc strikes the sample surface. The electrode holder is then moved across the sample's width, perpendicular to its length. In similar fashion, succeeding lines are set very close to each other. Using an ordinary pencil sharpener, the carbon rod is honed to a fine tip after every tenth line. This is repeated until both marked areas are adequately covered. The sample is then turned over and the backside is treated in exactly the same way.

Sandblasting is a common and proven technique to enhance emissive properties of a surface. The improvement of this optical characteristic is based on the surface roughness, which this technique produces. A sandblasting gun is connected to high-pressure air and a container filled with sand. Pulling a trigger allows the high-pressure air to pick up and accelerate sand particles to high velocities. Sand particles impact on the surface and alter the surface morphology. The sand is commercially available and has an average diameter of approximately 200 μm. High-velocity sand alters the sample in designated areas (analysis and experiment areas). These areas clearly exhibit a dull appearance when compared with untreated areas.

V. Experimental Results and Material Characterization

To determine the evolution of emissive properties, a total of 14 samples were tested during this study. Niobium and tantalum samples were subjected to two different surface-altering methods (namely, sandblasting and arc-texturing) and compared with the performance of untreated samples. Surface morphology plays a significant role with regard to radiative characteristics. The target temperature was 1700 K, because the objective of this study was to explore enhancement of (waste) heat ejection at significantly higher temperatures than current engineering practice. Arc-textured niobium and tantalum samples were also tested at a temperature of 1300 K to allow an assessment as a function of temperature. Arc-textured samples were subjected to different testing durations (namely, 4, 8, and 12 h) at these temperatures. This allowed the evaluation of macroscopic and microscopic changes in surface morphology as a function of time. Further, appraisal of starting conditions was made possible, which permits testimony regarding reproducibility of surface morphology by the prescribed arc-texturing procedure. After each heating experiment, the macroscopic appearance was documented photographically to aid later on in the analysis. To maintain clarity, diagrams in this section reflect experimental results achieved during the 12-h testing period. In the case of both arc-textured materials, emissivity values for shorter testing durations follow the trend and mimic the results very closely (within less then 3%) of the 12-h experiments. These results attest to excellent reproducibility of surface morphology during the arc-texturing process and provide high confidence in the experiment execution.

A. Experimental Evaluation of Total Emissivity

Figure 5 graphically illustrates the importance and significance of surface morphology. Operating the samples at a temperature of 1700 K, the graph compares the emitted power as a function of surface condition and time. Clearly, the ability to reject heat is significantly enhanced by altering the surface morphology. Sandblasting and arc-texturing augment the power amount of untreated samples by 160 and 275%, respectively. When comparing sandblasting and arc-texturing with each other, the power increase yields 170%. Further, it is evident that morphology changes take place during the testing period, which is apparent in the subtle decrease of emitted power at constant temperature. This morphology change for the sandblasted sample rapidly happens during the first 40 min after the startup period and then asymptotically approaches a stable value (namely, around 360 W). The arc-textured sample experiences a less dramatic power decay over an extended period of time, suggesting smaller morphological changes. Over the 12-h testing period, the emitted power decreased by 15% (equivalent to 100 W) and settled around a value of 570 W.

A summary of test results for total emissivity as a function of time, material, temperature, and surface morphology is provided in Fig. 6. Emissivity of untreated niobium and tantalum samples establish the baseline for comparison of altered surfaces. The smooth surface of tantalum and niobium achieve emissivities of about 0.25 and 0.35, respectively. Over the course of the testing period, these values remain stable and constant.

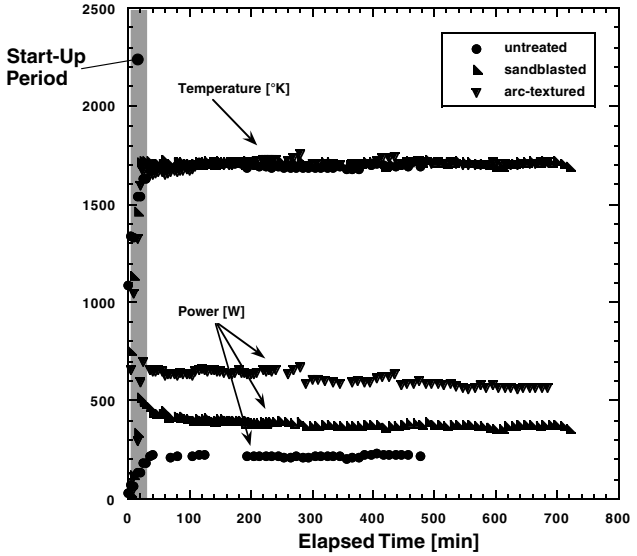

Fig. 5 Power as a function of time and surface condition at constant temperature (tantalum).

Rough-surface morphology strongly enhances the emissivity of materials, as numerous studies have demonstrated [28–30]. The degree of roughness has a significant influence on the emissivity as a function of time. Sandblasted samples exhibit a noticeable change in emissive ability during the testing period at 1700 K. The emissivity drops exponentially for both materials. Initial values for tantalum and niobium are 0.55 and 0.44, respectively. For tantalum, the gradient of the change is larger and change occurs over a longer period of time. Eventually, emissivities of both materials asymptotically approach a value of 0.4. Sandblasting considerably enhances emissive capabilities of tantalum with respect to the untreated sample. This particular surface-alteration technique yields a 160% improvement once a stable point is reached. Niobium adds a moderate increase of about 15%.

Surface conditions of arc-textured samples drastically improve radiative properties during testing at 1700 K. As with the sandblasted samples, arc-textured samples experience decay in emissivity during the testing period. Initial emissivities of both materials have a value of about 0.9 and then decrease exponentially to about 0.6. In both cases, the decay gradients change with time. During the initial phase of the heating, arc-texturing of niobium and tantalum weighed against smooth surfaces enhances the emissivity by 260 and 360%, respectively. At the termination point of the experiments, this enhancement still accounts for 170 and 240%. Over time, the ability to emit a set amount of power gradually decreases. Surface morphology changes, which are responsible for emissivity enhancement, occur more slowly when compared with sandblasted samples and manifest themselves in less drastic alterations. To maintain a constant testing temperature (namely, 1700 K), degradation of emissive ability implicates a reduction of electrical power input to the sample (Fig. 5).

During experiments conducted at 1300 K, radiative properties of arc-textured surfaces exhibit similar trends: namely, high emissivity and gradual decrease as a function of time. The initial emissivities for tantalum and niobium are 0.87 and 0.92, respectively. The arc-textured tantalum sample quickly reaches a constant value of about 0.83, and the emissivity for niobium asymptotically approaches a value of 0.84 through a subtle change in gradient. The lower testing temperature maintains emissivity values, which are 93% or better than the initial values at 1700 K.

B. Material Characterization

The second main objective of this study is to identify likely causes that contribute to the change of emissive characteristics and how these changes can be controlled to produce highly engineered surfaces with very specific attributes. Several material characterization techniques are applied to verify the likely causes of change in integrated radiative properties. Optical microscopy (OM), SEM, and stylus-type prolifometry are employed to study the geometric topology of altered surfaces. Energy-dispersive x-ray spectroscopy (EDS) and x-ray diffractometry (XRD) provide information on likely surface constituents produced during texturing processes. Combined, these techniques will assist in unlocking the mechanisms that are ultimately responsible for emissivity behavior as a function of time and temperature and that consequently lead to manufacturing processes of desirable morphologies.

1. Optical and Scanning Electron Microscopy

Figure 6 includes OM and SEM images obtained at different stages of the experiments correlating emissivity behavior and surface morphology. All OM images are taken at a magnification factor of 200× times and represent a typical region of the sample. The sequences of arc-textured niobium and tantalum tested at 1700 K are at a magnification of only 25× times, which was necessary to present a wider field of view. With regard to SEM, most images represent magnifications between 4250 and 4750×.

Before the heating experiments commence, a baseline of starting conditions is established for the three different surface morphologies (untreated, sandblasted, and arc-textured) of tantalum and niobium. To the naked eye, all surfaces have distinct features, which are magnified to allow a macroscopic description of surface morphology. Untreated samples of niobium and tantalum are smooth, shiny, and characterized by fine grooves obtained during the manufacturing process. Sandblasting produced a dull/diffuse appearance of the surface. Closer inspection with OM reveals a uniform distribution of in-and-out-of-focus areas over the field of view. Blurry parts are a result of height differences in surface structure, because the focus is fixed to one optical depth. Arc-texturing produces a dark appearance of the samples. During the procedure, metal from the surface and graphite from the electrode vaporize due to the high temperature in the arc. The vapor mixture then condenses onto the surface when the electrode is moved to another site. OM images show a black and pitted surface. Significant microscopic information is gained by SEM images of sandblasted and arc-textured surfaces. These morphologies have distinct features, which vastly differ from each other. Sandblasting produces a surface characterized by sharp edges that are reminiscent of a brittle shattered object. The impact of sand particles causes a rough morphology, which could be attributed to some degree to (probable) residue of fragmented sand particles. Arc-texturing produces microscopic spheres in a variety of sizes. These spheres appear alone or fused into clusters. As already mentioned, arc-texturing produces a vapor mixture of carbon and metal. Microscopic droplets form in the condensed mixture and instantly solidify on the surface. Random layering of spheres produces cavitylike features. SEM images reveal no new information regarding the surface morphology of untreated samples. Conditions of these different surface morphologies are shown in Fig. 6.

Images obtained after the heating experiments are benchmarked against those depicting starting conditions. Macroscopic and microscopic changes of physical features allow a correlation to the observed changes in emissivity as a function of time and temperature. With regard to these two variable parameters, two main conclusions are drawn through a careful analysis of experimental data and topological features: namely, the gradual loss of the black coating and the gradual change of morphological elements. From a macroscopic perspective, OM images of tantalum and niobium tested at 1700 K reveal a gradual diminishing of the black coating, whereas such optical change during the 1300 K testing is not discernible. The photo sequences in Fig. 6 show an intermixture of coated and bare metal surfaces and correlate this behavior with the achieved emissive performance after 4, 8, and 12 h. Lacking a coating completely, OM images of sandblasted tantalum and niobium exhibit the other source for changes in total emissivity. Compared with the starting conditions, larger fractions of examined areas are in focus. This indicates a decay in roughness height, which causes the emissivity to decrease as it is observed in the diagram of Fig. 6. As reported in the literature, this decrease of roughness causes lower emissivity, which eventually approaches smooth surface conditions.

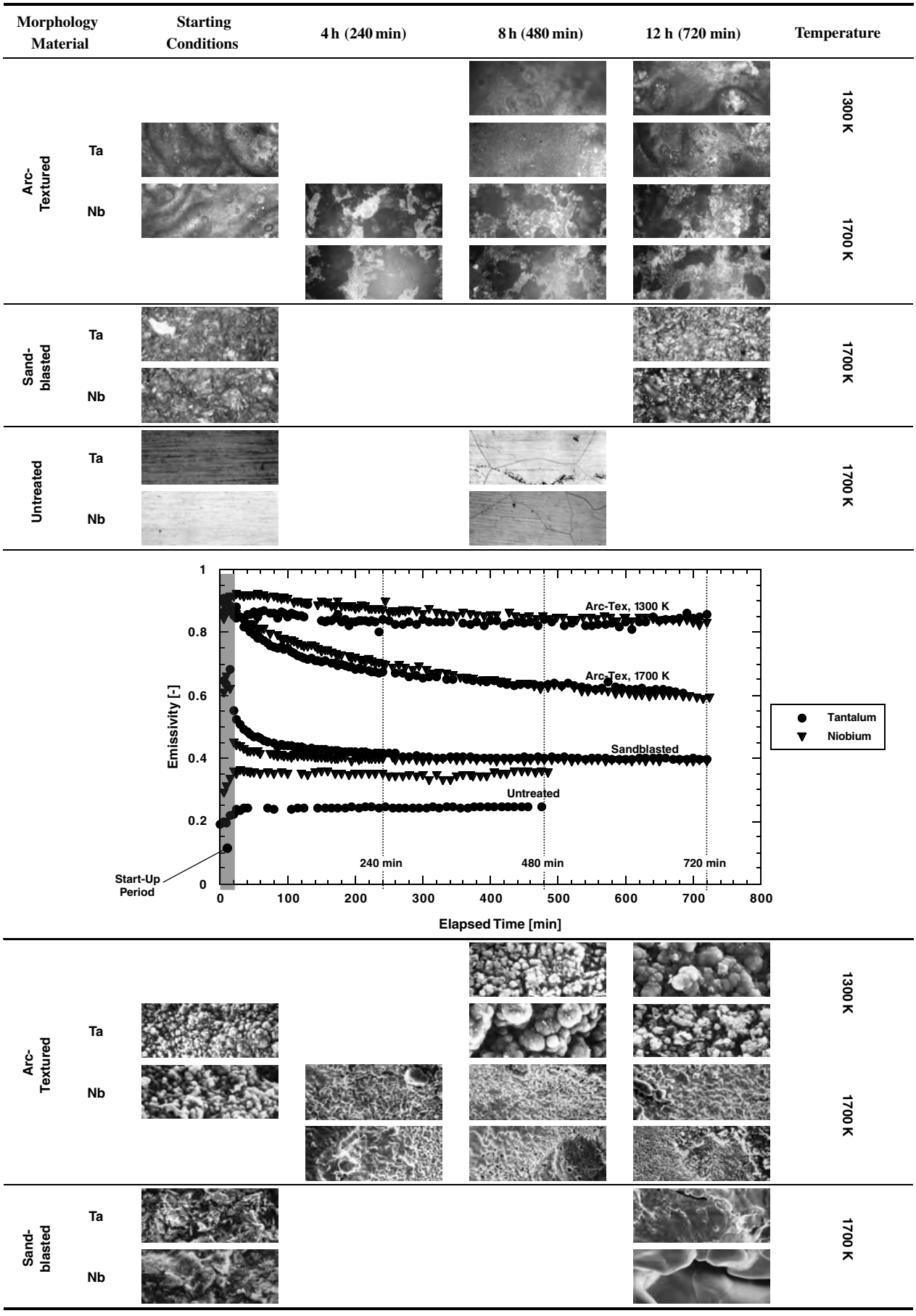

Fig. 6 Emissivity as a function of morphology, material, time, and temperature.

SEM images further confirm observations made on the macroscopic level. The microscopically fine defined features for sandblasted and arc-textured surfaces (as we have recorded them before the heating experiments) have undergone drastic changes as a function of time and temperature. Comparing before and after pictures of sandblasted surfaces reveals a very obvious difference in morphology. Sharp edges and peaks of various heights caused by the impact of sand particles have disappeared and are replaced by a morphology resembling a smoother surface. Even the grain structure is reemerging and visible. The macroscopic and microscopic roughness has declined with time and temperature, consequently causing a decrease in emissivity, as illustrated in Fig. 6. In areas in which the black coating has been lost, SEM pictures of arc-textured surfaces reveal a morphology similar to that observed with sandblasted surfaces after they were heated. These surfaces also approach near-smooth surface conditions. Moving the viewing site closer to the interface between coated and bare metal allows additional interesting observations and conclusions. The remaining coated areas do not differ in appearance from those observed before heating and are still characterized by spheres of various sizes. The morphology of the bare metal along the borderline with the coated area is characterized by fine structures. These structures appear to be the result of spheres fused together, because it occurs in the sintering process in which metal particles bond and partially fuse at temperatures below the melting point. As the distance from the borderline increases, these new features merge with the underlying bulk material and become less pronounced. The roughness established by the arc-texturing process changes due to the lack of black coating and diminishes with growing distance from the coated area. The sequence of SEM pictures for both metals tested at 1700 K eloquently illustrates these observations in Fig. 6. For this purpose, the pictures for niobium were taken at a magnification of about 1900× to provide a larger field of view. Viewing arc-textured samples with a neutral-density filter during testing at 1700 K revealed lighter and darker areas along the sample, which implies a variation in local temperature and spectral emissivity. Assuming a constant power output per area, the coated area emits that power at higher emissivity and lower temperature, and the bare surface compensates the lower emissivity with a higher temperature. The temperature difference of two adjacent areas could lead to thermal stress. Consequently, differences in thermal expansion coefficients lead to a graduated loss of coated areas and a demise in emissive capability.

2. Surface Roughness by Stylus-Type Prolifometry

Surface quality is an important property in many engineering applications. Surface roughness affects friction and many other mechanical properties. Optical properties of a surface are strongly influenced by its roughness. For this project, an analysis of surface roughness was performed with a DEKTAK IIA profilometer. The instrument provides the average roughness, which is expressed as the mean deviation of the height measurement. A diamond stylus with a radius of 12.5 μm scans the surface.

All samples were scanned with regard to material, morphology, test temperature, and duration. Analysis and a careful evaluation of the roughness data did not produce a pattern that could be correlated to the experimental results and the photographic analysis. Two main factors contributed to this finding: namely, the size of features contributing to roughness and the lack of pattern determining roughness distribution. Profilometer analyses are based on scanning at least one cross-sectional profile of a surface. The macroscopic features of arc-textured tantalum and niobium are highly irregular. Because the position of scanned surface profiles is arbitrary and random, the calculated average roughness need not necessarily represent the statistical roughness of the whole surface area. Further, the radius of the diamond stylus is significantly larger than the characteristic size of spheres on the surface of arc-textured materials. Figure 7 illustrates the stylus radius compared with macroscopic and microscopic features. The bar length represents the radius at the specific magnifications. The profilometer stylus is not capable of responding to the size of macroscopic and microscopic morphology achieved by either sandblasting or arc-texturing.

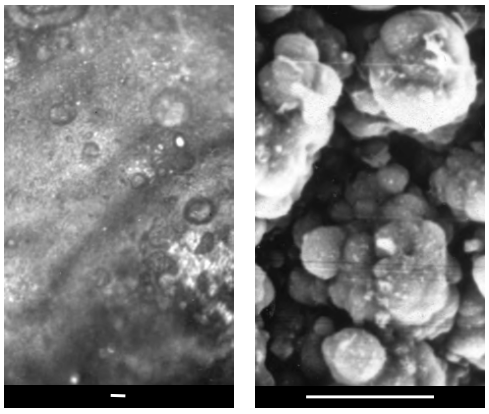

Fig. 7 Comparison of the stylus radius with the sizes of macroscopic and microscopic features.

3. Energy-Dispersive X-Ray Spectroscopy

The working principle of EDS is based on energy dispersion and collection of characteristic x rays. When atoms in a material are ionized by high-energy radiation, they emit characteristic x rays. EDS was employed to determine and evaluate the constituents on arc-textured surfaces. Because the surfaces appear black after the arc-texturing procedure, it is assumed that carbon is deposited in some way on the surface of the materials. During the texturing process, high temperatures in the arc vaporize bulk metal from the surface and carbon from the texturing electrode. Most likely, the vapor consists of carbon, host material (Ta and Nb), carbon-metal compounds, and impurities. After moving the electrode to another site, the vapor condenses on the surface, leaving a thin deposition of a high-emissivity material. This layer was identified as the cause of enhanced radiative properties. Figure 8 shows the histogram for niobium and tantalum. The analyzing software detected carbon, niobium, and tantalum, respectively. No other elements were identified. EDS analyses confirm the assumption that the black

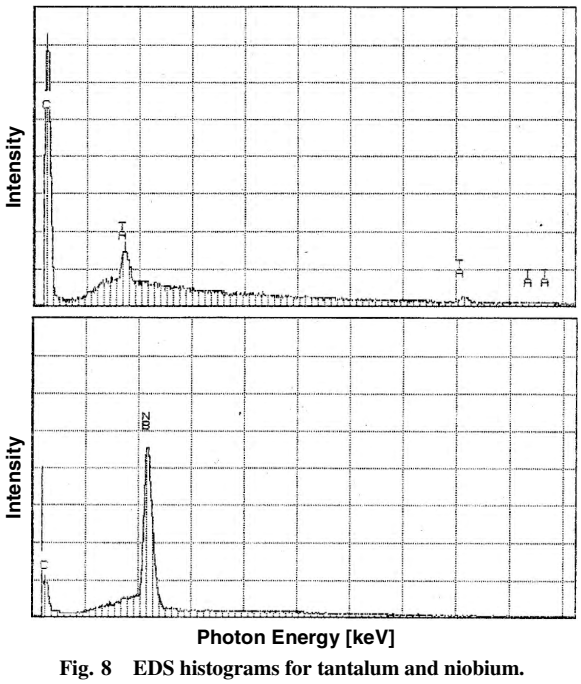

Fig. 8 EDS histograms for tantalum and niobium.

appearance of the surface is due to carbon deposition. Carbon and graphite achieve an emissivity that is two–nine times higher than the emissivity of metals. It is responsible for the increased and strongly enhanced radiative properties of radiator materials.

4. X-Ray Diffractometry

EDS analyses only provided information on the elements presence, but were not conclusive about compound composition. Two possibilities have to be considered: namely, carbide compounds with the bulk material and/or amorphous carbon embedded in the surface. XRD identifies crystalline phases, which are present at the surface of a material. Furthermore, this powerful technique gives information about the structural properties of these phases. They include strain state, grain size, phase composition, and defected structures. XRD is used to determine the thickness of thin films and multilayers, as well as the atomic arrangements in amorphous materials and interfaces. EDS analyses indicated carbon in the surface of arc-textured materials; however, EDS information is limited to element detection and concentration. The diffraction patterns of arc-textured niobium and tantalum were compared against the Joint Committee on Powder Diffraction Standards (JCPDS) database. The JCPDS software identified niobium carbide, niobium oxide nitride, tantalum carbide, and tantalum oxide. Oxide compounds of both materials are probably formed during the arc-texturing procedure. Some oxygen remained in the enclosure during the discharge treatment. It is also conceivable that the surface oxidized after the procedure, because the samples were not stored in an inert-gas environment. XRD analyses revealed metal and carbon compounds in the deposited layer. No crystalline carbon such as graphite or diamond was found in the layer.

VI. Conclusions

The main objectives of this study were to evaluate emissive properties at high temperatures of materials for which the surface was altered by arc-texturing and to determine the mechanisms that are responsible for the enhancement of emissive capabilities. The study incorporated and employed a multitude of diagnostic methods to aid in correlating experimental data with physical properties. Electric arc discharge treatment of surfaces depends on various parameters. The morphology achieved by the particular set of parameters chosen for this study demonstrated promising performance with regard to operating temperatures. The emissivity shows significant improvement at operating temperatures of 1300 and 1700 K when weighted against untreated surfaces. At these conditions, emissive capability diminishes as a function of operating time, especially at the higher test temperature. The study revealed important insights regarding the mechanisms accountable for the observed behavior of emissivity as a function of time and temperature. Contributing features are a thin coating of carbon and carbon compounds coexisting with a microscopically rough surface. The scope of the study did not include an investigation to increase the stability of the coating and to consequently secure retainment of this crucial morphology, which is so imperative to the success of arc-textured surfaces.

Arc-texturing is an effective method for altering surface morphology and, as such, for producing engineered, highly integrated, surfaces with desirable emissive properties. Because the nature and behavior of this method are sensitive to multiple parameters, additional work needs to done to fully develop, assess, and promote its potential.

Acknowledgments

This work was supported by the Strategic Defense Initiative Organization and Office of Innovative Science and Technology (SDIO/TNI) through contract DNA 001-90-C-0127. The author wishes to thank M. Frank Rose (Radiance Technologies, Inc.) and Steve Best (Space Research Institute, Auburn University). Further, the author is indebted to the Auburn University Department of Poultry Science and Department of Chemistry and Biochemistry for assistance and help in using and obtaining data with the scanning electron microscopy and x-ray diffraction facilities. The author also wishes to express gratitude to the electrophysics branch at NASA John H. Glenn Research Center at Lewis Field for obtaining measurements of surface roughness.

References

[1] Mikellides, I. G., Jongeward, G. A., Schneider, T., Peterson, T., Kerslake, T. W., and Snyder, D., "Solar Arrays for Direct-Drive Electric Propulsion: Electron Collection at High Voltages," *Journal of Spacecraft and Rockets*, Vol. 42, No. 3, 2005, pp. 550–558. doi:10.2514/1.5609

[2] Malone, P. K., and Williams, G. T., "Lightweight Inflatable Solar Array," *Journal of Propulsion and Power*, Vol. 12, No. 5, 1996, pp. 866–872.

[3] Brandhorst, H., Rodiek, J., O'Neill, M., and Eskenazi, M., "Ultralight, Compact, Deployable, High-Performance Solar Concentrator Array for Lunar Surface Power," AIAA Paper 2006-4104, June 2006.

[4] Reid, C. M., Smart, M. C., Bugga, R. V., Manzo, M. A., Miller, T. B., and Gitzendanner, R., "Performance and Comparison of Lithium-Ion Batteries Under Low-Earth-Orbit Mission Profiles," NASA TM-2007-214826, Dec. 2007.

[5] Burke, K., "Fuel Cells for Space Science Applications," AIAA Paper 2003-5938, Aug. 2003.

[6] Mason, L. S., "A Power Conversion Concept for the Jupiter Icy Moons Orbiter," *Journal of Propulsion and Power*, Vol. 20, No. 5, 2004, pp. 902–910. doi:10.2514/1.5805

[7] Frisbee, R. H., "Advanced Space Propulsion for the 21st Century," *Journal of Propulsion and Power*, Vol. 19, No. 6, 2003, pp. 1129–1154.

[8] Incropera, F. P., and DeWitt, D. P., *Introduction in Heat Transfer*, Wiley, New York, 1981.

[9] Dever, J., Deshpande, M., Jaworske, D., and Cerbus, C., "Issues and Advancements in Space Durable Multi-Functional Thermal Control Coatings," *Proceedings of the Space Technology and International Forum (STAIF)*, edited by E. G. Mohamed, AIP Conference Proceedings 813, American Inst. of Physics, Melville, NY, 2006, pp. 3–10.

[10] Jaworske, D. A., "A Review of Textured Surfaces, Paints, and Coatings for Space Radiator Applications," *Proceedings of the Space Technology and International Forum (STAIF)*, edited by, E. G. Mohamed, AIP Conference Proceedings 699, American Inst. of Physics, Melville, NY, 2004, pp. 71–75.

[11] Jaworske, D. A., "Emittance Characterization of Thermal Control Paints, Coatings, and Surfaces Using a Calorimetric Technique," *Thin Solid Films*, Vol. 253, Nos. 1–2, 1994, pp. 233–237. doi:10.1016/0040-6090(94)90326-3

[12] Jaworske, D. A., "Thermal Modeling of a Calorimetric Technique for Measuring the Emittance of Surfaces and Coatings," *Thin Solid Films*, Vol. 236, Nos. 1–2, 1993, pp. 146–152. doi:10.1016/0040-6090(93)90660-H

[13] Dever, J. A., Rutledge, S. K., and Mayer, K., "Atomic Oxygen/Vacuum Ultraviolet Radiation Exposure of Z-93 and Z-93-P Coatings," AIAA Paper 1996-0148, Jan. 1996.

[14] DeGroh, K. K., Roig, D. M., Burke, C. A., and Shah, D. R., "Performance and Durability of High Emittance Heat Receiver Surfaces for Solar Dynamic Power Systems," NASA TM-106549, Mar. 1994.

[15] Feig, J., "Radiator Concepts for High Power Systems in Space," AIAA Paper 1984-0055, Jan. 1984.

[16] Edgerton, R. H., and Diem-Kirsop, P. D., "Liquid Droplet Radiator Thermal Characteristics," AIAA Paper 1986-1162, June 1986.

[17] Bankoff, S. G., Griffing, E. M., and Schluter, R. A., "Use of an Electric Field in an Electrostatic Liquid Film Radiator," *Annals of the New York Academy of Sciences*, Vol. 974, 2002, pp. 1–9.

[18] Tagliafico, L. A., and Fossa, M., "Lightweight Radiator Optimization for Heat Rejection in Space," *Heat and Mass Transfer*, Vol. 32, 1997, pp. 239–244. doi:10.1007/s002310050117

[19] Frisbee, R., and Hoffman, N., "SP-100 Nuclear Electric Propulsion for Mars Cargo Missions," AIAA Paper 1993-2092, June 1993.

[20] Rose, M. F., Hyder, K., Askew, R. F., Chow, L., Gilmour, A. S., and Faghri, A., "Novel Techniques for the Thermal Management of Space-Based, High-Power Microwave Tubes," *IEEE Transactions on Electron Devices*, Vol. 38, No. 10, Oct. 1991, pp. 2252–2263.

[21] Edwards, D. K., and Catton, I., "Radiation Characteristics of Rough and Oxidized Metals," *Advanced Thermophysical Properties at Extreme Temperature and Pressure (SERGE GRATCH)*, American Society of Mechanical Engineers, New York, 1965, pp. 189–199.

[22] Thomas, L. K., "Thermal Radiation from Rough Tungsten Surfaces in Normal and Off-Normal Directions," *High Temperature*, Vol. 6, Jan.–June 1968.

[23] Mahan, J. R., Kowsary, F., and Eskin, L. D., "Apparent Emissivity of Conical and Cylindrical Cavities: Comparison of Monte Carlo and Exact Analytical Results," *Radiation, Phase Change Heat Transfer, and Thermal Systems*, Vol. 81, Heat Transfer Div., American Society of Mechanical Engineers, New York, 1987.

[24] Kaufman, H. R., and Robinson, R. S., "Ion-Beam Texturing of Surfaces," *Journal of Vacuum Science and Technology*, Vol. 16, No. 2, Mar./Apr. 1979, pp. 175–178.

[25] Mirtich, M. J., and Kussmaul, M. T., "Enhanced Thermal Emittance of Space Radiators by Ion-Discharge Chamber Texturing," NASA TM-100137, 1987.

[26] Banks, B. A., Rutledge, S. K., Mirtich, M. J., Behrend, T., Hotes, D., Kussmaul, M., Barry, J., Stidham, C., Stueber, T., and DiFilippo, F., "Arc-Textured Metal Surfaces for High Thermal Emittance Space Radiators," NASA TM-100894, 1988.

[27] Richmond, J. C., and Harrison, W. N., "Equipment and Procedures for Evaluation of Total Hemispherical Emittance," *American Ceramic Society Bulletin*, Vol. 39, 1960, pp. 668–73.

[28] Proteus, J. O., "Relation between the Height Distribution of a Rough Surface and the Reflectance at Normal Incidence," *Journal of the Optical Society of America*, Vol. 53, No. 12, 1963, pp. 1394–1402.

[29] Caren, R. P., and Liu, C. K., "Thermal Radiation from a Microscopically Roughened Dielectric Surface," *Journal of Heat Transfer*, Vol. 94, No. 1, Feb. 1972, pp. 73–79.

[30] Birkebak, R. C., Sparraw, E. M., Eckert, E. R. G., and Ramsey, J. W., "Effect of Surface Roughness on the Total Hemispherical and Specular Reflectance of Metallic Surfaces," *Journal of Heat Transfer*, Vol. 86, No. 2, May 1964, pp. 193–199.

J. Minow
Associate Editor